ChemComm

COMMUNICATION

View Article Online
View Journal | View Issue

Check for updates

Cite this: *Chem. Commun.*, 2022, **58**, 3689

Received 14th December 2021,
Accepted 7th February 2022

DOI: 10.1039/d1cc07030d

rsc.li/chemcomm

Published on 08 February 2022. Downloaded on 12/4/2025 9:18:56 PM.

Concerted effect of Ni-in and S-out on ReS_2 nanostructures towards high-efficiency oxygen evolution reaction†

Tapas K. Das,[a] Tapan Ping,[ab] Manoj Mohapatra,[cd] Shahid Anwar,[a] Chinnakonda S. Gopinath[e] and Bikash Kumar Jena *[ab]

Herein, a one-step hydrothermal reaction is developed to synthesize a Ni-doped ReS_2 nanostructure with sulphur defects. The material exhibited excellent OER activity with a current density of 10 mA cm^{-2} at an overpotential of 270 mV, a low Tafel slope of 31 mV dec^{-1}, and good long-term durability of 10 h in 1 M KOH. It shows high faradaic efficiency of 96%, benefiting from the rapid charge transfer caused by the concerted effect of Ni-in and S-out on the ReS_2 nanostructure.

Hydrogen has received significant attention to boost green and sustainable energy growth as an alternative to fossil fuels and the associated severe environmental pollution problems.[1–3] Water electrolysis is considered promising, eco-friendly, and one of the best ways to produce hydrogen. It has two complementary half-reactions, *i.e.*, the hydrogen evolution reaction (HER) at the cathode and the oxygen evolution reaction (OER) at the anode. However, the efficiency of the overall water splitting process gets circumscribed by the sluggish kinetics of the OER, it being a complicated multistep four-electron transfer process.[3–5] Therefore, catalysts are needed to increase the reaction rate and lower the overpotentials towards the OER. Ru and Ir-based materials are currently the benchmark catalysts for the OER, but their shortage and high-cost limit their commercialization and industrial production.[6,7] So, it is necessary to develop an electrocatalyst of abundant elements with high activity and durability with low cost. Recently, earth abundant transition metal di-chalcogenide (TMD) compounds have attracted tremendous attention due to their cost-effectiveness and outstanding ability toward catalytic HER and OER activity.[8]

TMDs such as ReX_2 (X = S, Se) have emerged and received great attention due to their surprising structural, electrical, optical, and chemical properties. Generally, TMDs are stabilized in a highly symmetric 2H structure, but ReX_2 is a distorted trigonal 1T phase system with shrunk in-plane crystal symmetry.[9] Several 2D TMDs have been constructed by doping, alloying, heteroatom incorporation, and vacancy creation as a blueprint for better electrolytic performance. Similar to other 2D TMDs, the catalytic activity of ReS_2 also comes from the edge sites, whereas the basal planes have very poor activity. So stimulating the basal planes would be a promising approach for increasing the catalytic activity of the ReS_2-based materials. Recent theoretical studies have suggested that doping of transition metals on 1T′ ReS_2 can increase the active sites on the basal planes.[10,11] Recently, a few reports have revealed the intrinsic HER activity of ReS_2-based materials. However, the OER properties of the ReS_2 structure have not been explored thoroughly. This report portrays the synthesis of Ni-doped and S-vacancy ReS_2 nanostructures by hydrothermal and wet chemical methods. A study of the concerted effect of Ni-in and S-out on the ReS_2 nanostructures towards the OER is performed (Fig. 1). Here, Ni doping at different percentages with S vacancies at different durations on ReS_2 nanostructures has been optimized and used for OER applications. The material with 5% Ni doping and S vacancies is referred to as $Ni_d(5)S_v@ReS_2$ NS. Fig. S1 (ESI†) shows the X-ray diffraction (XRD) pattern of the $Ni_d(5)S_v@ReS_2$ NS material. It shows five peaks located at 2θ values of 14.04°, 21.42°, 32.88°, 46.7°, and 57.79°, corresponding to the (100), (101), (002), (1$\bar{1}$3) and ($\bar{1}$22) diffractions of the distorted triclinic ReS_2 (JCPDF No. 82-1379).[12] Fig. S2 (ESI†) shows the SEM image of the $Ni_d(5)S_v@ReS_2$ NS material. It consists of a hierarchical structure assembled from many nanosheet ReS_2 layered structures. From the elemental color mapping, it is inferred that Re, S, and Ni are evenly distributed over the whole samples (Fig. S2, ESI†). The high-resolution transmission electron microscope (HR-TEM)

[a] *Materials Chemistry Department, CSIR-Institute of Minerals and Materials Technology, Bhubaneswar, Odisha, 751013, India. E-mail: bikash@immt.res.in*
[b] *Academy of Scientific & Innovative Research, Ghaziabad, 201002, India*
[c] *Radiochemistry Division, Bhabha Atomic Research Centre, Trombay, Mumbai, 400085, India*
[d] *Homi Bhabha National Institute, Anushakti Nagar, Mumbai, 400094, India*
[e] *Catalysis and Inorganic Chemistry Division, CSIR-National Chemical Laboratory, Dr Homi Bhabha Road, Pune, 411008, India*

† Electronic supplementary information (ESI) available: Experimental details, characterization and electrochemical analysis. See DOI: 10.1039/d1cc07030d

Published on 08 February 2022. Downloaded on 12/4/2025 9:18:56 PM.

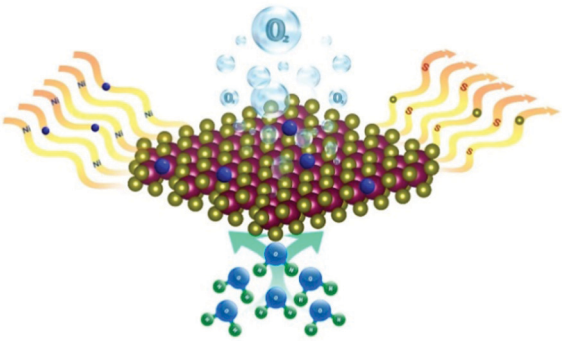

Fig. 1 Scheme showing the concerted effect of Ni-in and S-out on ReS_2 nanostructures towards the OER.

images are shown in Fig. S3 (ESI†); they represent the homogeneous spherical structures consisting of a large number of ultrathin nanosheets. It is observed that ultrathin nanosheets are assembled as seen from the HR-TEM image (Fig. S3, ESI†). The lattice fringes are visible from the HR-TEM images, and the lattice spacing of 0.274 nm can be assigned to the (002) plane of the ReS_2 (Fig. 2(a)). The SAED pattern signifies the crystalline nature of the material (inset of Fig. S3, ESI†). X-ray photoelectron spectroscopy (XPS) was employed to investigate the chemical compositions and electronic environment on the surface of the samples. The survey scan spectrum shows the presence of different elements (Fig. S4, ESI†). The Ni doping is also established from the presence of Ni 2p in the spectra. The Re 4f spectra can be deconvoluted into four peaks with peak maxima at binding energies of 42.00, 44.50, 45.90, and 48.0 eV; those at 42.00 and 44.50 eV can be assigned to the Re $4f_{7/2}$ and Re $4f_{5/2}$, respectively, of Re^{4+} in the ReS_2 (Fig. 2(b)).[13] The other peaks located at 45.90 and 48.0 eV can be ascribed to the Re $4f_{7/2}$ and Re $4f_{5/2}$ of Re^{7+}, respectively.[14] The existence of Re^{7+} can be ascribed to the adsorption of the precursor, ReO_4^- ions on the surface of the materials.[15] The S 2p spectra were also resolved into two

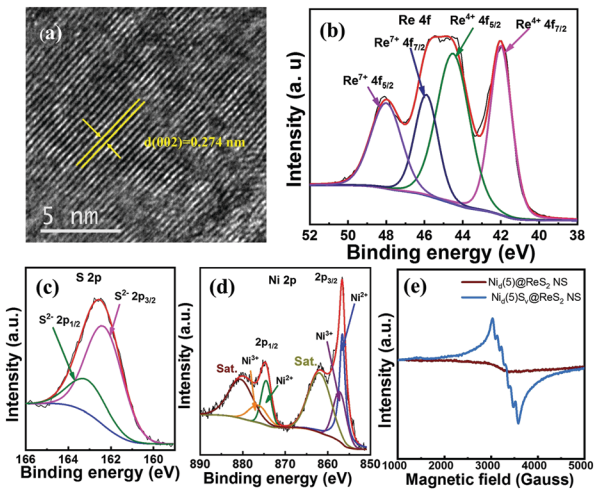

Fig. 2 (a) HRTEM image of $Ni_d(5)S_v@ReS_2$ NS. Deconvoluted fine XPS spectra of $Ni_d(5)S_v@ReS_2$ NS: (b) Re 4f, (c) S 2p and (d) Ni 2p. (e) EPR spectra of $Ni_d(5)S_v@ReS_2$ NS and $Ni_d(5)@ReS_2$ NS.

corresponding peaks (Fig. 2(c)). The peaks located at 162.4 and 163.5 eV ensure the presence of $2p_{3/2}$ and $2p_{1/2}$ levels of S^{2-}, respectively.[16,17] The core level of the Ni 2p spectrum is shown in Fig. 2(d), and can be deconvoluted into two doublets and two shakeup satellites. The peaks located at binding energies of 856.6 and 874.1 eV are ascribed to $2p_{3/2}$ and $2p_{1/2}$ core levels of Ni^{2+}, respectively. Whereas the peaks at 857.2 and 875.3 eV are due to the presence of $2p_{3/2}$ and $2p_{1/2}$ for Ni^{3+}.[18] The other two broad peaks at 862.0 and 881.3 eV are the satellite peaks associated with the corresponding main peaks. The existence of Ni^{3+} is mainly due to the slight oxidation of Ni on the surface. The room temperature electron paramagnetic resonance (EPR) spectra of the samples with and without sulphur vacancies were measured to investigate the dangling bonds and the nature of the sulphur vacancies present in the samples (Fig. 2(e)). The *g* factors for both the samples are calculated and are found to be 2.21 and 2.018 for $Ni_d(5)@ReS_2$ and $Ni_d(5)S_v@ReS_2$ NS, respectively. It is found that the $Ni_d(5)@ReS_2$ NS sample without S vacancies showed very weak EPR intensity, and the signal may be due to the background cavity. In contrast, the $Ni_d(5)S_v@ReS_2$ NS exhibited a highly intense EPR signal, supporting the presence of the unpaired electrons and proving the defect creation *via* S vacancies.[19] The other low-intensity peaks may be due to the Re-related local defects arising from dangling bonds or dislocation due to the presence of Ni.

The concerted effect of Ni-in and S-out in $Ni_d(5)S_v@ReS_2$ NS towards the OER properties has been demonstrated. The electrocatalytic OER activity of $Ni_d(5)S_v@ReS_2$ NS modified on a glassy carbon (GC) electrode was demonstrated using linear sweep voltammetry (LSV) at a 5 mV s^{-1} scan rate in a three-electrode system, using 1 M KOH. Similar measurements were performed on blank GC and the benchmark catalysts IrO_2/C and commercial RuO_2 for comparison. The corresponding polarization curves are presented in Fig. 3(a). It is observed that, after Ni doping into the ReS_2 system, the OER activity and the oxygen-evolving current density increased remarkably compared to its undoped ReS_2 counterpart. The OER activity is further enhanced by introducing S vacancies on it. $Ni_d(5)S_v@ReS_2$ NS shows only 270 mV overpotential (η) to reach a current density of 10 mA cm^{-2}, whereas $Ni_d@ReS_2$ NS exhibited 327 mV. It is observed that the $Ni_d(5)S_v@ReS_2$ NS delivers quite enhanced activity compared to the benchmark catalysts IrO_2/C (η_{10}@297 mV) and RuO_2 (η_{10}@380 mV). The overpotentials of the materials at a current density of 10 and 20 mA cm^{-2} are presented in a radar plot (Fig. 3(b)). This signifies that the concerted effect of Ni-in and S-out in $Ni_d(5)S_v@ReS_2$ NS increases the OER activity. The Tafel plots were obtained from the corresponding polarisation curves and their slopes were evaluated to understand the reaction kinetics of the as-synthesized catalysts (Fig. S5, ESI†). The $Ni_d(5)S_v@ReS_2$ NS shows the lowest Tafel slope value of 31 mV dec^{-1} among the studied samples and this Tafel slope value is significantly lower than that of IrO_2/C, suggesting that the $Ni_d(5)S_v@ReS_2$ NS has faster reaction kinetics for the OER. It is worth comparing the OER activity of $Ni_d(5)S_v@ReS_2$ NS with the other reported metal sulphides and the results are summarized in Table S1 (ESI†). However, very few reports demonstrate the OER

 This journal is © The Royal Society of Chemistry 2022

Published on 08 February 2022. Downloaded on 12/4/2025 9:18:56 PM.

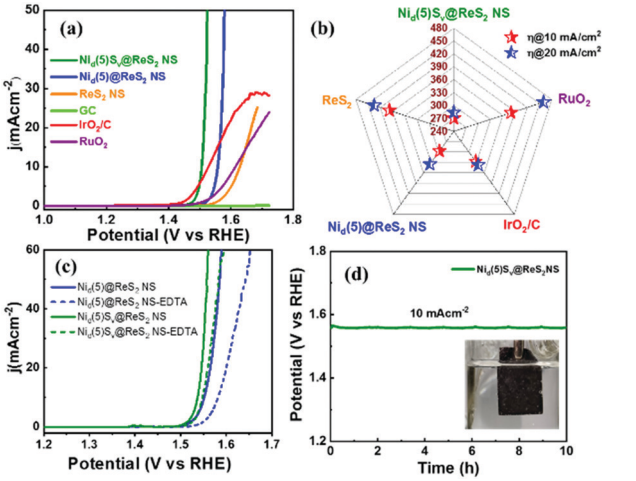

Fig. 3 (a) The OER LSV polarisation plots of the materials, (b) radar plot showing the comparison of the overpotentials, (c) LSV polarisation plots with and without EDTA and (d) chronopotentiometric long term stability test (inset shows the image of O_2 generation).

activity of ReS_2-based materials. For example, Pang *et al.* developed sulphur defect-rich ReS_2 by annealing at a high temperature (700 °C) with an H_2/N_2 environment and studied the OER activity.[14] They revealed the OER overpotential of 290 mV at a current density of 10 mA cm^{-2} and Tafel slope value of 81 mV dec^{-1}. Majidi *et al.* developed ReS_2 by chemical vapour transport methods and studied the OER activity in an aprotic solvent.[20] They exhibited the highest current density of 6.89 mA cm^{-2}, which signifies that the OER activity is remarkably lower compared to the activity in 1 M KOH. Tian *et al.* reported a high OER activity of 280 mV overpotential at 10 mA cm^{-2} current density for Fe-doped NiS_2/MoS_2 composites.[8] Huang *et al.* developed mesoporous CoS/MoS_2 heterointerfaces and reported a good OER activity of 281 mV (η_{10}).[21] The above comparison justifies that the material in the present report, Ni$_d$(5)S$_v$@ReS_2 NS, provides a simple wet-chemical development process and shows promising OER activity. It is well established that the OER proceeds through four consecutive reaction steps, and the metal centres mostly act as the active sites. A catalytic poisoning test was carried out to detect the catalytically active metal centres in the catalyst. Ethylenediaminetetraacetate (EDTA) has a very high binding efficiency with metal centres, suppressing their activity. 1 mM EDTA solution in 1 M KOH electrolyte was used to study the involvement of the catalytically active metal centres of Ni$_d$(5)S$_v$@ReS_2 NS for the OER. The results show that the OER activity significantly reduced by shifting to higher overpotential and with a decrease in current density (Fig. 3(c)). This observation suggests that EDTA binds with the active metal centres and blocks the metal-active sites for the OER mechanism. So, the superior OER activity for the Ni$_d$(5)Sv@ReS_2 NS arises due to the presence of a metal-active centre in the catalyst. The long-term stability of the catalyst was also recorded by the chronopotentiometric method at a fixed current density of 10 mA cm^{-2} for 10 h in 1 M KOH (Fig. 3(d)). The Ni$_d$(5)S$_v$@ReS_2 NS exhibits very steady potentiometric curves with almost 98% overpotential retention over 10 h of continuous operation. The XRD, HRTEM and XPS analyses have been carried out for Ni$_d$(5)S$_v$@ReS_2 NS after the long-term stability test (Fig. S6–S8, ESI†). The XRD shows some characteristic peaks of Ni$_d$(5)S$_v$@ReS_2 NS (Fig. S6, ESI†). The careful analysis of the HRTEM images shows the possible presence of (1$\bar{1}$0) of $Ni(OH)_2$ and (110) of Ni–OOH (Fig. S7, ESI†). The hydroxide and oxy-hydroxides present at the Ni centres on the surface of the catalyst are the possible OER active sites and are responsible for the excellent OER activities. Also, this observation is further supported by the XPS analysis, the peak intensity for Ni^{3+} is enhanced compared to Ni^{2+} suggesting the possible formation of Ni–OOH (Fig. S8(b), ESI†). The satellite peak area and intensity of Ni are significantly enhanced compared to the pristine catalyst, indicating the formation of a surface oxide layer.[22,23] This analysis suggests that the catalyst transformed into a metal hydroxide and oxy-hydroxide of Ni and this is responsible for the enhancement of the OER activity.[24,25] The OER performance was optimized at different concentrations of Ni doping on ReS_2, and the activity of the catalysts is presented in Fig. S9 (ESI†). It has been observed that on increasing the doping from 1% to 5%, the OER overpotential (@10 mA cm^{-2}) decreases from 360 mV to 327 mV. Further increasing the Ni doping (10%) requires a higher overpotential of 355 mV to catalyze the OER process. Therefore, 5% Ni doping on ReS_2 (Ni$_d$(5)@ReS_2 NS) is used for developing S vacancies. The effect of saturation time for the creation of S vacancies on Ni$_d$(5)@ReS_2 NS was investigated at different times of chemical treatment (10, 20, 30, and 60 min) with $NaBH_4$, and the OER performance was verified (Fig. S10, ESI†). It was observed that Ni$_d$(5)@ReS_2 NS treated for 30 min (Ni$_d$(5)S$_v$@ReS_2 NS) showed better OER activity with lower overpotential. A rotating ring disk electrode (RRDE) experiment was performed in 1 M KOH at a rotating speed of 1600 rpm to confirm the formation of oxygen bubbles through the OER catalytic process.[26] The generation of O_2 bubbles at the disk electrode was inferred by an increase in the ring current due to the oxygen reduction reaction (ORR) polarisation curves at the ring electrode while applying a constant potential of 1.5 V *vs.* RHE at the disk electrode (Fig. 4(a)). From the OER polarisation curve, when the potential was scanned from 1.2 V to 1.7 V, there is a very small but significant current (~5 μA) generated at the ring electrode compared to the disk electrode (Fig. 4(b). This suggests that the water oxidation follows the four-electron pathway on the catalyst surface of Ni$_d$(5)S$_v$@ReS_2 NS. The OER faradaic efficiency was estimated from the RRDE experiment (Fig. 4(c)) using eqn (S9) (ESI†) to illustrate that the current generated at the disk is from the water oxidation reactions only. After applying a constant current of 300 μA at the disk electrode for oxygen generation, about 57.6 μA was observed at the ring electrode. This suggests a high faradaic efficiency (FE) of 96% for the OER catalyst Ni$_d$S$_v$@ReS_2 NS. The intrinsic activity of the synthesized electrocatalyst was further analyzed by the electrochemical double-layer capacitance (C_{dl}), relative electrochemical active surface area (ECSA), turnover frequency (TOF), mass activity (MA), and charge transfer resistance (R_{ct}) (Fig. S11–S13, ESI†) and the respective parameters are summarised in Table S2 (ESI†). It has been observed that Ni$_d$(5)S$_v$@ReS_2 NS exhibits the highest C_{dl} value of 0.15 μF cm^{-2}, a large relative ECSA of 3.4, a lower R_{ct} value

Published on 08 February 2022. Downloaded on 12/4/2025 9:18:56 PM.

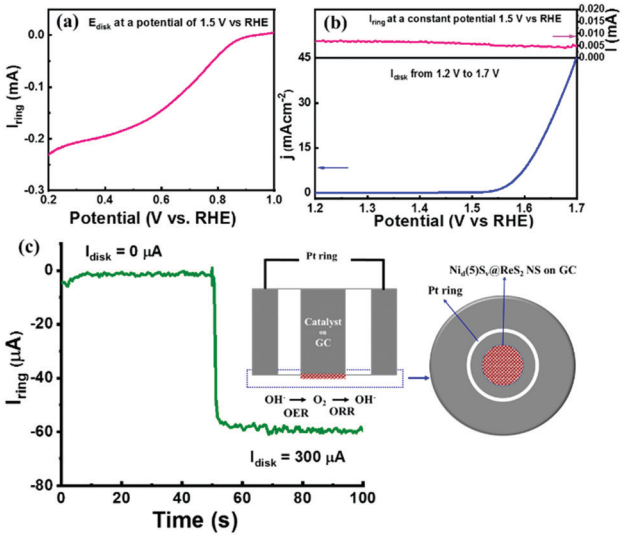

Fig. 4 (a) RRDE LSV plot of $Ni_d(5)S_v$@ReS_2 NS showing the ORR on the ring electrode at a disk potential of 1.5 V (*vs.* RHE), (b) OER LSV plot on the disk electrode measuring the current response on the ring electrode and (c) faradaic efficiency (FE) calculation using the RRDE techniques (inset shows the FE testing mechanism and RRDE configuration).

of 52.64 Ω, a high mass activity of 122, and a reasonably good TOF of 0.409 s^{-1} (@300 mV overpotential) compared to other samples in this study. The higher number of active sites is responsible for the superior OER activity, supported by the large C_{dl} and ECSA values. Furthermore, the current density of LSV plots is normalized to the relative ECSA values to find the intrinsic OER activities without the influence of surface area (Fig. S14, ESI†). It is observed that $Ni_d(5)S_v$@ReS_2 NS delivers a higher current density than $Ni_d(5)$@ReS_2 NS and ReS_2 NS, which suggests that the OER mechanism follows the involvement of a surface oxide-rich activation layer.[24] The possible elemental dissolution has been investigated by comparing the C_{dl} values before and after the long-term stability test (Fig. S15, ESI†) and ICP-OES analysis (ESI†). The observations support the high stability towards long-term use.[27] The continuous O_2 effervescence from the catalyst over the GC plate (Video S1, ESI†) suggests that the $Ni_d(5)S_v$@ReS_2 NS can open up a new paradigm for realistic OER applications.

In summary, we have presented the successful synthesis of Ni-doped and sulphur vacant ReS_2 nanosheets as a highly efficient OER electrocatalyst *via* a very facile hydrothermal and chemical etching method. The as-prepared $Ni_d(5)S_v$@ReS_2 NS electrocatalyst could deliver a current density of 10 mA cm^{-2} at a small overpotential of 270 mV, with a small Tafel slope of 31 mV dec^{-1} and good durability with a high faradaic efficiency of 96%. The presence of S vacancies and Ni doping is characterized by the EPR and XPS analysis. This work provides a highly effective and stable electrocatalyst for OER applications and opens up a promising and straightforward strategy to develop catalysts for other applications.

T. K. D. and T. P. acknowledge CSIR, India for the fellowship, and B. K. J. thanks CSIR, UGC CSR, BRNS, and MNRE, India for financial support.

Conflicts of interest

There are no conflicts to declare.

References

1 W. Li, Q. Shen, D. Men, Y. Sun, W. Cao, J. Y. Lee, B. Kang, Y. Sun and C. Li, *Chem. Commun.*, 2021, **57**, 1774–1777.
2 C. S. Gopinath and N. Nalajala, *J. Mater. Chem. A*, 2021, **9**, 1353–1371.
3 B. Mohanty, P. Bhanja and B. K. Jena, *Mater. Today Energy*, 2021, **23**, 100902.
4 F. Qin, D. Zhou, M. Sun, W. Xu, H. Tang, J. Fan and W. Chen, *Chem. Commun.*, 2021, **57**, 11561–11564.
5 S. Mondal, B. Mohanty, M. Nurhuda, S. Dalapati, R. Jana, M. Addicoat, A. Datta, B. K. Jena and A. Bhaumik, *ACS Catal.*, 2020, **10**, 5623–5630.
6 L. Gao, X. Cui, C. D. Sewell, J. Li and Z. Lin, *Chem. Soc. Rev.*, 2021, **50**, 8428–8469.
7 P. Guha, B. Mohanty, R. Thapa, R. M. Kadam, P. V. Satyam and B. K. Jena, *ACS Appl. Energy Mater.*, 2020, **3**, 5208–5218.
8 J. Tian, X. Xing, Y. Sun, X. Zhang, Z.-G. Li, M. Yang and G. Zhang, *Chem. Commun.*, 2022, **58**, 557–560.
9 X. Li, C. Chen, Y. Yang, Z. Lei and H. Xu, *Adv. Sci.*, 2020, **7**, 2002320.
10 J. Pan, R. Wang, X. Xu, J. Hu and L. Ma, *Nanoscale*, 2019, **11**, 10402–10409.
11 J. Xu, C. Fang, Z. Zhu, J. Wang, B. Yu and J. Zhang, *Nanoscale*, 2020, **12**, 17045–17052.
12 F. Qi, Y. Chen, B. Zheng, J. He, Q. Li, X. Wang, B. Yu, J. Lin, J. Zhou, P. Li and W. Zhang, *J. Mater. Sci.*, 2017, **52**, 3622–3629.
13 J. Gao, L. Li, J. Tan, H. Sun, B. Li, J. C. Idrobo, C. V. Singh, T. M. Lu and N. Koratkar, *Nano Lett.*, 2016, **16**, 3780–3787.
14 Q. Q. Pang, Z. L. Niu, S. S. Yi, S. Zhang, Z. Y. Liu and X. Z. Yue, *Small*, 2020, **16**, 1–10.
15 S. Liu, Y. Liu, W. Lei, X. Zhou, K. Xu, Q. Qiao and W. H. Zhang, *J. Mater. Chem. A*, 2018, **6**, 20267–20276.
16 P. Devaraji, M. Mapa, H. M. A. Hakkeem, V. Sudhakar, K. Krishnamoorthy and C. S. Gopinath, *ACS Omega*, 2017, **2**, 6768–6781.
17 M. Chauhan, K. P. Reddy, C. S. Gopinath and S. Deka, *ACS Catal.*, 2017, **7**, 5871–5879.
18 Z. Li, Y. Xu, X. Ren and W. Wang, *J. Mater. Sci.*, 2020, **55**, 13892–13904.
19 L. Li, Z. Qin, L. Ries, S. Hong, T. Michel, J. Yang, C. Salameh, M. Bechelany, P. Miele, D. Kaplan, M. Chhowalla and D. Voiry, *ACS Nano*, 2019, **13**, 6824–6834.
20 L. Majidi, Z. Hemmat, R. E. Warburton, K. Kumar, A. Ahmadiparidari, L. Hong, J. Guo, P. Zapol, R. F. Klie, J. Cabana, J. Greeley, L. A. Curtiss and A. Salehi-Khojin, *Chem. Mater.*, 2020, **32**, 2764–2773.
21 W. H. Huang, X. M. Li, X. F. Yang, H. Bin Zhang, F. Wang and J. Zhang, *Chem. Commun.*, 2021, **57**, 4847–4850.
22 C. L. Wang, C. Q. Song, W. H. Shen, Y. Y. Qi, Y. Xue, Y. C. Shi, H. Yu and L. Feng, *Catal. Sci. Technol.*, 2019, **9**, 1769–1773.
23 P. Luo, H. Zhang, L. Liu, Y. Zhang, J. Deng, C. Xu, N. Hu and Y. Wang, *ACS Appl. Mater. Interfaces*, 2017, **9**, 2500–2508.
24 Y. Yuan, S. Adimi, X. Guo, T. Thomas, Y. Zhu, H. Guo, G. S. Priyanga, P. Yoo, J. Wang, J. Chen, P. Liao, J. P. Attfield and M. Yang, *Angew. Chem., Int. Ed.*, 2020, **59**, 18036–18041.
25 S. Jin, *ACS Energy Lett.*, 2017, **2**, 1937–1938.
26 B. Mohanty, Y. Wei, M. Ghorbani-Asl, A. V. Krasheninnikov, P. Rajput and B. K. Jena, *J. Mater. Chem. A*, 2020, **8**, 6709–6716.
27 S. Hirai, T. Ohno, R. Uemura, T. Maruyama, M. Furunaka, R. Fukunaga, W. T. Chen, H. Suzuki, T. Matsuda and S. Yagi, *J. Mater. Chem. A*, 2019, **7**, 15387–15394.

 This journal is © The Royal Society of Chemistry 2022